PHYSICAL REVIEW B VOLUME 25, NUMBER 1 1 JANUARY 1982

Electron-spin-resonance study of $Pb^- 6p^3$ in KCl: A possible Jahn-Teller system

Etienne Goovaerts
Physics Department, University of Antwerp (U.I.A.), B-2610 Wilrijk, Belgium

Sergiu Nistor
Central Institute of Physics, I.F.T.M., C.P. 5206, Bucuresti, Romania

Dirk Schoemaker
Physics Department, University of Antwerp (U.I.A.), B-2610 Wilrijk, Belgium

(Received 30 March 1981)

Four $S=\frac{1}{2}$ electron-spin-resonance spectra exhibiting orthorhombic symmetry ($[1\bar{1}0]$, [001], [110]) and observed in KCl:Pb^{2+} after x irradiation at temperatures above 220 K are identified as originating from Pb^- centers. The mobility of the anion and cation vacancies above this temperature is shown to be essential in the production of these defects. The Pb^- spectra are characterized by strongly anisotropic g values ranging from ~ 0.7 to ~ 4 and their explanation requires a coupling scheme for Pb^- intermediate between LS and j-j and a full diagonalization of the crystal field, the spin-orbit interaction, and the Coulomb repulsion between the 20 states of the p^3 configuration. A comparison is made between the crystal fields experienced by $Pb^- 6p^3$ and by the previously studied LS-coupled system $Sn^- 5p^3$. Because of the sizable presence of orbital angular momentum in its Γ_8 ground state, the Pb^- is shown to induce a static Jahn-Teller distortion when occupying an unperturbed octahedral anion site. The Jahn-Teller energies are estimated to be $\sim 10^3$ cm^{-1} for Pb^-, and ~ 10 cm^{-1} for Sn^-. It is concluded that the orthorhombic symmetry in all four Pb^- defects is caused by a static Jahn-Teller distortion of mixed E_g and T_{2g} character and that vacancies, if present, merely exert an additional perturbation. This viewpoint is shown to be a fruitful one: It allows us (i) to explain the near constancy throughout the four defects of the dominant crystal-field parameter ($\sim -2\times 10^4$ cm^{-1}) and (ii) to propose specific models for two of the Pb^- centers.

I. INTRODUCTION

In alkali halides doped with certain positive metal ion impurities it has proved possible to produce the corresponding negative metal ions by a suitable treatment. The production procedures employed so far involve either additive or electrolytic coloring. A series of negative metal ion defects which are reasonably well characterized are the ns^2 ($n=4, 5, 6$) species Cu^-,[1] Ag^-,[2,3] and Au^- (Refs. 4–6) produced in several Cu^{2+}-, Ag^+-, and Au^+-doped alkali halides. The identification of these negative ions was based on the strong similarities that exist between their optical properties (absorption, luminescence, circular dichroism, etc.) and those of the corresponding isoelectronic ns^2 ($n=4, 5, 6$) positive metal ion impurities Ga^+, In^+, and Tl^+ which had already been extensively investigated.[7]

The existence in several alkali halides of[8–11] Pb^-, Sn^-, Ge^-, and[12–14] Tl^- ions has also been claimed. This identification was based on various optical and electrical conductivity measurements, but the interpretation of the data is difficult and not always convincing. In fact, the complete absence of electron-spin-resonance (ESR) signals and of circular dichroic effects possessing a temperature dependence appropriate for paramagnetic defects[15] strongly argues against the existence of the paramagnetic np^3 species Pb^-, Sn^-, and Ge^- in electrolytically or additively colored specimens. As a result models involving nonmagnetic aggregates of these negative metal ions have been put forward.[16]

Recently[17] Sn^- ($5p^3\,{}^4S$) ions were unambiguously identified by ESR techniques in KCl:Sn^{2+} samples which have been x irradiated at room temperature (RT). These Sn^- ions occurred under the form of several complex defects involving, besides the Sn^- on a negative ion site, one or more perturbing entities (primarily anion and cation vacancies) in the immediate vicinity. Extensive measurements showed that next to suitable electron trapping properties for Sn^{2+}, Sn^+, and Sn^0 (i.e., a sufficient electron affinity aided or not by the Madelung field) the mobility above 220 K of the cation vacancy but especially the anion vacancy was of crucial importance in the production of the Sn^- defects. The cation vacancies are present in the crystal as charge compensators for the Sn^{2+}, while the anion vacancies are produced by the x irradiation together with halogen interstitials.[18]

The present paper discusses the KCl:Pb^{2+} system in which after x irradiation at RT we have also observed the ESR spectra of several complex $Pb^- 6p^3$ defects. It will be shown in Secs. III and IV that the analysis and interpretation of the Pb^- ESR data are nontrivially different from the Sn^- analysis[17] and that this has two related causes: First, the much larger spin-orbit interaction leads to a coupling scheme for the free Pb^- ion intermediate between *LS* and *j-j* (the former described rather well the Sn^- case) and, second, the influence of the environment is described by a strong effective crystal field which mixes substantial amounts of excited states into the Pb^- ground state. This results in effective *g* factors very much different from the value 2. Section V presents data on production by x irradiation and discusses some thermal and photochemical properties. Again the mobility above 220 K of the anion and cation vacancies is found to be of crucial importance in the formation of the complex Pb^- defects. Finally, in Sec. VI an attempt is presented to propose precise microscopic models for these Pb^- centers. It will be argued, because of the strong orbital angular momentum presence in the degenerate Pb^- ground state, that the symmetry of the Pb^- centers is determined primarily by a dominant orthorhombic static Jahn-Teller (JT) distortion.

II. EXPERIMENTAL

The Pb^{2+}-doped crystals used in most of these experiments were grown by the Bridgman method in quartz ampoules filled with chlorine gas. The starting materials were very pure KCl (CERAC) with a low Br^- content (~ 10 ppm) and 0.17 mol% of ultrapure $PbCl_2$ (VENTRON). In preliminary experiments crystals were used which were grown in air by the Kyropoulos method from a reagent-grade KCl melt containing 1 wt.% of $PbCl_2$. Besides a lower lead content and the presence of O_2^- centers, no differences with the Bridgman-grown samples were observed in the ESR spectra. Samples containing the ^{207}Pb isotope with 92% enrichment were also available. These samples also contained a somewhat lower lead concentration and exhibited traces of O_2^-.

The x irradiations were performed from 77 K upward using a Siemens tube with a tungsten target and operating at 50 kV and 50 mA. Prior to the x irradiation the KCl:Pb^{2+} samples were heated to about 400 °C for several minutes and then quickly cooled to RT or lower. By this treatment aggregates of Pb^{2+}—positive-ion-vacancy complexes are dissolved. Further details on sample handling, x irradiations, ESR instrumentation, and optical excitation procedures can be found in Refs. 17–19.

III. ANALYSIS OF THE Pb^- ESR SPECTRA

As we shall demonstrate in Sec. IV the ESR spectra that will be described originate from defects each involving a single Pb^- ion. We shall anticipate this already in the nomenclature and call the defects $Pb^-(1)$, $Pb^-(2)$, $Pb^-(3)$, and $Pb^-(4)$.

The $Pb^-(1)$ and $Pb^-(2)$ centers are conveniently produced by a 15-min x irradiation of a KCl:Pb^{2+} specimen at room temperature. The $Pb^-(3)$ and $Pb^-(4)$ defects require the following production sequence. A KCl:Pb^{2+} crystal is irradiated at 250 K for 15 min, is then warmed to room temperature for about 15 min (in the dark), and is finally excited with *F*-center light at ~ 15 K. The resulting ESR spectra recorded at 15 K are presented in Fig. 1. In the region between 0.40 and 0.70 T one discerns Pb^+ ESR spectra[20] which will not be discussed in this paper. The narrow region around $g \approx 2$ (≈ 0.33 T) contains Pb^{3+},[21] $BrCl^-$, and Cl_2^- lines.[22] The remaining narrow lines originate from the Pb^- defects. These ESR spectra are characterized by single strongly anisotropic lines flanked by weaker doublets down in intensity by a factor of ~ 8. These lines originate from defects each involving a single Pb nucleus: The strong single lines are attributed to the even-*A* Pb isotopes

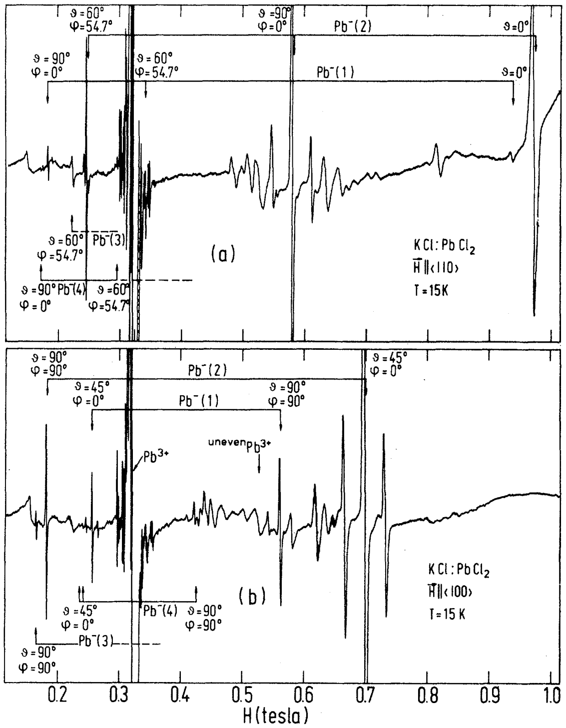

FIG. 1. ESR spectra at 15 K of the Pb^- centers produced in KCl:$PbCl_2$ crystals by a 20-min x irradiation at 260 K (see Fig. 8) for (b) $\vec{H} \parallel \langle 100 \rangle$ and (a) $\vec{H} \parallel \langle 110 \rangle$. The microwave frequency is $\nu = 9.16$ GHz.

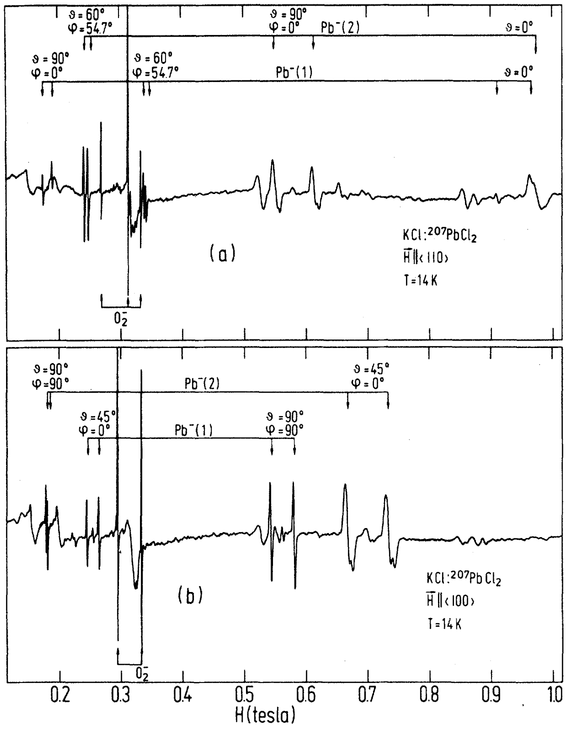

FIG. 2. ESR spectra at 14 K of the Pb^-(1) and Pb^-(2) centers clearly showing the ^{207}Pb doublet hyperfine splitting in KCl:$^{207}PbCl_2$ crystals containing 92% enriched ^{207}Pb. The sample had been x irradiated for 20 min at room temperature (see Figs. 8 and 9). The microwave frequency is $\nu = 9.16$ GHz.

(^{204}Pb, ^{206}Pb, and ^{208}Pb together are 79% abundant) which possess no nuclear spin, while the doublets originate from hyperfine interaction of the unpaired electrons with the ^{207}Pb nuclei (21% abundant) which possess nuclear spin $\frac{1}{2}$ and a nuclear moment $\mu_N(^{207}Pb)$ = 0.5837 nuclear magnetons.

Experiments using KCl crystals doped with 92% enriched $^{207}PbCl_2$ substantiate the correctness of this interpretation: The ESR spectra now exhibit strong doublets with a much weaker (by a factor of ~ 4.5) line in the center. These spectra are shown in Fig. 2.

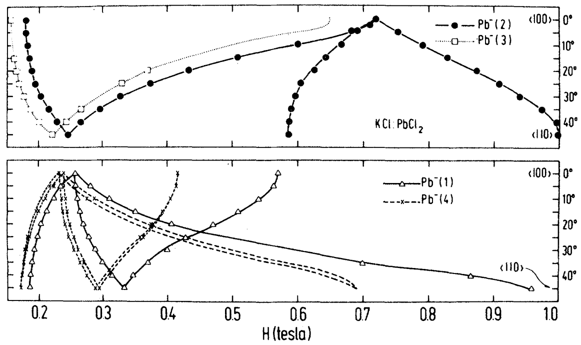

FIG. 3. Angular variation of the Pb^- ESR spectra in KCl:$PbCl_2$ at $\nu = 9.16$ GHz. The magnetic field was rotated in a {100} plane.

An angular variation study of the Pb^- defects is shown in Fig. 3. It is clear from these figures that three defects possess orthorhombic symmetry with a set of axes (x,y,z) being, e.g., $[1\bar{1}0]$, [001], and [110], respectively. The Pb^-(4) center also possesses orthorhombic symmetry but its z axis is tilted 0.8° away from [110] in a (001) plane. In Figs. 1 and 2 the resonance lines are labeled by the polar angles (ϑ, φ) which define the direction of the static external field $\vec{H}$ with respect to the set of axes (x,y,z).

The ESR spectra were fitted to an $S = \frac{1}{2}$ spin Hamiltonian (usual notation),

$$H/g_0\mu_B = g_0^{-1}\vec{H}\cdot\overline{\overline{g}}^{\text{eff}}\cdot\vec{S} + \vec{S}\cdot\overline{\overline{A}}(\text{Pb})\cdot\vec{I} \ , \qquad (1)$$

and the results are presented in Table I.

Inspection of this table shows that the sets of g components of all centers are comparable to one another, but there is one remarkable difference: the g values corresponding to the $y \parallel [001]$ and $x \parallel [1\bar{1}0]$ directions are interchanged in going from Pb^-(1) and

TABLE I. The experimental ESR parameters of the Pb^- defects in KCl ($T = 15$ K). The hyperfine parameters, A, and the reduced linewidths $\Delta H = (g^{\text{eff}}/g_0)\Delta H^{\text{expt}}$ are given in milliteslas.

Defect	g_x^{eff} $[1\bar{1}0]$	g_y^{eff} [001]	g_z^{eff} [110]	A_x^{eff} $[1\bar{1}0]$	A_y^{eff} [001]	A_z^{eff} [110]	ΔH
Pb^-(1)	3.555 ± 0.003	1.151 ± 0.001	0.6857 ± 0.0006	23.8 ± 0.1	25.0 ± 0.1	18.8 ± 0.1	1.7 ± 0.1
Pb^-(2)	1.114 ± 0.001	3.668 ± 0.003	0.6595 ± 0.0006	4.0 ± 0.1	35.6 ± 0.1	< 5[a]	2.3 ± 0.1
Pb^-(3)	. . . [b]	4.033 ± 0.003	. . . [b]	. . .	. . .	. . .	3.0 ± 0.1
Pb^-(4)[c]	3.792 ± 0.003	1.546 ± 0.001	0.9458 ± 0.0008	< 2[a]	18.8 ± 0.1	. . .	2.0 ± 0.1

[a] Estimated from the broadening of the ESR lines when going from the natural to the ^{207}Pb enriched isotope.

[b] The g_x^{eff} and g_z^{eff} values could not be measured, but only $g^{\text{eff}}(\theta = 60°, \phi = 54.7°) = 2.938 \pm 0.002$.

[c] The x and z axes are tipped away from ⟨110⟩ in a {100} plane by a tippling angle $\theta_t = 0.80° \pm 0.02°$.

$\mathrm{Pb}^-(4)$ on the one hand to $\mathrm{Pb}^-(2)$ and $\mathrm{Pb}^-(3)$ on the other hand. When appropriate we will call $\mathrm{Pb}^-(1)$ and $\mathrm{Pb}^-(4)$ the Pb^- (I)-type centers and similarly $\mathrm{Pb}^-(2)$ and $\mathrm{Pb}^-(3)$ the Pb^- (II)-type centers.

The observed linewidth ΔH^{expt} is given by $\Delta H^{\mathrm{expt}} = (g_0/g^{\mathrm{eff}})\,\Delta H$, where ΔH is the true inhomogeneous or reduced linewidth. Because the g factor is strongly anisotropic, the observed linewidth is strongly anisotropic: The low-field lines (high g values) are much narrower than the high-field lines (low g values) as is indeed observed in Figs. 1 and 2. It is seen that the Pb^- linewidths are somewhat larger than the Sn^- linewidths $[\Delta H(\mathrm{Sn}^-) = 1.8\ \mathrm{mT}]$ and that the Pb^- (II)-type linewidths are distinctly broader than the ones of the Pb^- (I)-type centers.

The Pb^- ESR spectra are most strongly observed around 15 K. All of them possess similar saturation behavior: a slight saturation is observed below 15 K at microwave powers of about 50 mW. Increasing the temperature leads to a reduction in line intensity and to small shifts in the line positions, but no broadening of the lines is observed which might indicate the onset of motional effects.

IV. IDENTIFICATION AS Pb^-

A. Elimination procedure

It is clear by comparing the four sets of ESR parameters in Table I with each other that the same lead species must be involved in all four defects. By following a similar elimination procedure as employed for the Sn^- defects,[17] one can with a high probability identify this lead species with Pb^-.

First, the lead species cannot be a $\mathrm{Pb}^0\ 6p^2$. This even-electron system would yield an $S=1$ or 0 ground state neither of which is compatible with the observed $S=\frac{1}{2}$ ESR spectra. Second, the defects cannot contain Pb^+ ($6p^1\,{}^2P$) or Pb^{3+} ($6s^1\,{}^2S$). Such ions have been observed by ESR in x-irradiated $\mathrm{KCl{:}Pb}^{2+}$ crystal, and the ESR parameters are, for Pb^+,[20]

$$g_\parallel \cong 1.63,\quad A_\parallel({}^{207}\mathrm{Pb}) \cong 162.5\ \mathrm{mT}\ ,$$

$$g_\perp \cong 1.33,\quad A_\perp({}^{207}\mathrm{Pb}) \cong 256.4\ \mathrm{mT}\ ,$$

and, for Pb^{3+},[21]

$$g = 2.034,\quad A({}^{207}\mathrm{Pb}) = 11.8\ \mathrm{T}\ .$$

Both sets of parameters are very much different from the ones given in Table I.

A final possibility, namely, a linear molecule in a ${}^2\Pi$ ground state and involving a single Pb nucleus must also be discounted. The g components obtainable from such a system are g(parallel to axis) $=4$ and g(perpendicular to axis) $\equiv 0$ for the free molecule ion, whereas a crystal field of sufficiently low symmetry will push both g components towards the value 2. The data of Table I cannot be fitted to such a behavior and this is confirmed by a more quantitative analysis.

Thus, for all the above mentioned possibilities the g components in Table I cannot be explained. One is left with $\mathrm{Pb}^-\ 6p^3$ as the only alternative.

We will show in the following that Pb^- is indeed the species underlying the four Pb^- defects. This implies, just as for Sn^-,[17] that the Pb^- ion occupies an anion site and consequently, apart from trapping three electrons, the lead must have switched positions from a cation site (for Pb^{2+}) to an anion site (for Pb^-). Such a switching requires mobile anion vacancies and because these only occur above 220 K (Refs. 17, 23, and 24) Pb^- defects should only be producible by at least one x irradiation above 220 K. In Sec. V this will be shown to be the case.

B. Application of the Sn^- ($5p^3\,{}^4S$) analysis

The $\mathrm{Pb}^-\ 6p^3$ ion is, ignoring closed shells, isoelectronic with $\mathrm{Sn}^-\ 5p^3$ whose ESR spectra in $\mathrm{KCl{:}Sn}^{2+}$ crystals have been discussed at length in Ref. 17. A p^3 configuration yields in the LS coupling scheme the terms ${}^2D$, ${}^2P$, and ${}^4S$ of which the latter is the ground-state term. In a cubic crystal field the $J \equiv S = \frac{3}{2}$ degeneracy is not lifted and the ESR spectrum should consist of a single isotropic line (apart from hyperfine effects) around $g=2$. One of the observed Sn^- spectra was indeed a single isotropic line at $g \approx 1.97$ and the corresponding center was called Sn^- (cubic). The other Sn^- spectra were strongly anisotropic. One was axial from a center called Sn^-(tetrag), and the other two possessed orthorhombic symmetry and the corresponding defects were called Sn^-(ortho, 1) and Sn^-(ortho,2). All these Sn^- ESR spectra were accurately described by an $S=\frac{3}{2}$ spin Hamiltonian of the form (usual notation)

$$H/g_0\mu_B = D(S_z^2 - \tfrac{1}{3}\vec{S}^2) + E(S_x^2 - S_y^2) + g_0^{-1}\vec{H}\cdot\overleftrightarrow{g}\cdot\vec{S} \tag{2}$$

in which the D and E crystal field terms are much stronger than the Zeeman term. Such a situation yields two Kramers doublets whose calculated expressions for the g components accurately describe the strongly anisotropic Sn^- ESR spectra.

The lowest Kramers doublet can be described by a $S=\frac{1}{2}$ spin Hamiltonian of the form

$$H = \mu_B \vec{H}\cdot\overleftrightarrow{g}^{\mathrm{eff}}\cdot\vec{S}\ , \tag{3}$$

and in Ref. 17 it was demonstrated that (2) and (3) are related by

$$\begin{aligned} g_x^{\mathrm{eff}} &= g_x[1 \pm (1-3\alpha)(1+3\alpha^2)^{-1/2}]\ ,\\ g_y^{\mathrm{eff}} &= -g_y[1 \pm (1+3\alpha)(1+3\alpha^2)^{-1/2}]\ ,\\ g_z^{\mathrm{eff}} &= g_z[1 \mp 2(1+3\alpha^2)^{-1/2}]\ , \end{aligned} \tag{4}$$

in which the upper and lower sign apply to the cases $D > 0$ and $D < 0$, respectively. Only the absolute value of the g values can be determined experimentally.

Because Pb$^-$ is isoelectronic with Sn$^-$, it is selected for study with the same analysis.

Trying now to fit the g factors of Table I to expressions (4) yields unsatisfactory results: no good quantitative fit can be obtained. A crude approximate fit assuming $g_x = g_y = g_z = g$ yields

$$g \cong 1.45, \quad \alpha \cong 0.45 \quad .$$

The $g \approx 1.45$ result is particularly surprising in view of the fact that we are supposedly dealing with a ^4S state which possesses no orbital degeneracy. For Sn$^-$ the very reasonable $g \cong 1.97$ had been found. Taking an anisotropic $\overleftrightarrow{g}$ tensor in (4) does not improve the fit.

However, the $g \approx 1.45$ value is close to $g_J = \frac{4}{3}$, the atomic Landé factor of a $p_{3/2}$ orbital in the j-j coupling scheme. A p^3 configuration does indeed yield a $(p_{1/2})^2 p_{3/2}$ sequence in j-j coupling. This suggests that the LS-coupling approximation is a bad one for Pb$^-$ and that j-j or at least an intermediate coupling scheme is more appropriate.

Such an approach makes the $g \approx 1.45$ value acceptable, but the problem of a quantitative fit of the experimental g^{eff} components remains acutely the same: a $J = \frac{3}{2}$ state in crystal field or suitably low symmetry yields exactly the same expressions as given in (4) for the g^{eff} components. Thus an effective $S = \frac{3}{2}$ formalism fails no matter what coupling scheme is used.

C. Calculation of the g values of a Pb$^-$ ion in a strong crystal field

1. Description of the model calculation

As was pointed out in the foregoing subsection, it is not possible to obtain the g^{eff} parameters of the Pb$^-$ defects (see Table I) from an $S = \frac{3}{2}$ formalism, even if a weakly anisotropic $\overleftrightarrow{g}$ tensor is allowed in Eqs. (2) and (4). Both the Pb$^-$ and Sn$^-$ ion possess a p^3 ground-state configuration. However, Pb$^-$ is a heavier atom than Sn$^-$, and its spin-orbit coupling constant ξ is expected to be much larger than the Sn$^-$ one. In fact it is estimated in Sec. IV C 3 that $\xi(\text{Pb}^-) \cong 6100\ \text{cm}^{-1}$ whereas $\xi(\text{Sn}^-) \cong 1500\ \text{cm}^{-1}$. The LS-coupling scheme was found to be quite suitable for the Sn$^-$ case.[17] In this approximation the crystal-field terms in (2) are present only because the spin-orbit coupling induces a small admixture of $^2P_{3/2}$ states into the $^4S_{3/2}$ ground level. This admixture accounts for the shift between the observed $g = 1.97$ Sn$^-$ value and the $g_0 = 2$ free-electron value. Matrix elements of the crystal field between ^4S on the one hand and the excited ^2D and ^2P levels on the other are negligible.

For Pb$^-$, a coupling scheme intermediate between LS coupling and j-j coupling must be applied. The total spin S is not a good quantum number anymore and the ground state acquires a sizable orbital angular momentum. As a result, a crystal field can now have large matrix elements between the ground and the excited levels of the free ion. The $S = \frac{3}{2}$ description with spin Hamiltonian (2) becomes inadequate: All of the states of the $6p^3$ configuration must be taken into account in the calculation of the $\overleftrightarrow{g}^{\text{eff}}$ tensor of a Pb$^-$ ion in a strong crystal field. If the crystal field is weakened to such an extent that the admixture of excited levels in the ground state can be neglected, the $S = \frac{3}{2}$ formalism can be applied with an isotropic g value equal to the free Pb$^-$ g value (which is calculated to be 1.71 later in this section).

The g^{eff} parameters of the Pb$^-$ defects were calculated using the following model. The nonrelativistic p orbitals,

$$p_m = R_{6p}(r)\, V_{1m}(\theta, \phi), \quad m = 0, \pm 1 \quad , \tag{5}$$

with common radial function $R_{6p}(r)$, are used to build the 20 Slater determinants defined by the three equivalent p electrons. The calculation is conveniently performed in the LS-coupled base denoted by $|LSM_LM_S\rangle$ in which, as usual, L, M_L and S, M_S are the quantum numbers for the total orbital angular momentum $\vec{L}$ and the total spin $\vec{S}$ of the electrons. This base can be classified into three LS manifolds: ^4S, ^2D, and ^2P.

The following Hamiltonian is considered:

$$\mathcal{H}(\text{Pb}^-) = V_{e-e} + V_{\text{s.o.}} + V_c \quad , \tag{6}$$

consisting of the Coulomb repulsion between the electrons

$$V_{e-e} = \sum_{i>j}^{1,2,3} \frac{e^2}{r_{ij}} \quad , \tag{7a}$$

the spin-orbit coupling

$$V_{\text{s.o.}} = \xi \sum_{i=1}^{3} \vec{l}_i \cdot \vec{s}_i \quad , \tag{7b}$$

and the crystal-field term

$$V_c = -e \sum_{i=1}^{3} v_c(\vec{r}_i) \quad . \tag{7c}$$

The standard symbols are used for the electron charge, $-e$, the interelectronic distance, r_{ij}, and the one-electron orbital ($\vec{l}_i$) and spin ($\vec{s}_i$) momenta. Additional terms in the Hamiltonian such as the kinetic energy and the central potential of the ion, which are constant for all of the states of the $6p^3$ configuration, have no influence on our calculation and were omitted in (6).

The Coulomb repulsion term V_{e-e} is diagonal in the base $|LSM_LM_S\rangle$, with the following diagonal elements[25]:

$$\text{in } {}^4S,\ F_0-15F_2\ ;$$

$$\text{in } {}^2D,\ F_0-6F_2\ ;$$

$$\text{in } {}^2P,\ F_0\ ,$$

where F_0 and F_2 are the Slater-Condon parameters. In an *LS*-coupling approximation the average term splitting would be $6F_2$ to $9F_2$. The constant term F_0 will not be considered hereafter. The calculation of the matrix elements of $V_{\text{s.o.}}$ is straightforward as is shown in Ref. 25.

Figure 4 presents, on the left-hand part, an energy level scheme calculated in this model for the free Pb^- ion. The specific values of the parameters ξ and F_2 used in this calculation are discussed in the following subsection. The states are labeled by *J*, the total angular momentum of the free ion. Both in the limit of pure *LS* and of pure *j-j* coupling one can investigate which level gives a dominant contribution to the Pb^- eigenstates. This is indicated between brackets for each *J* level in Fig. 4. For the one-electron crystal-field potential v_c, an expansion in spherical harmonics around the lead nucleus is taken:

$$-e v_c(\vec{r}) = \sum_{l,m} A_{l,m} r^l Y_{lm}(\theta,\phi)\ ,$$

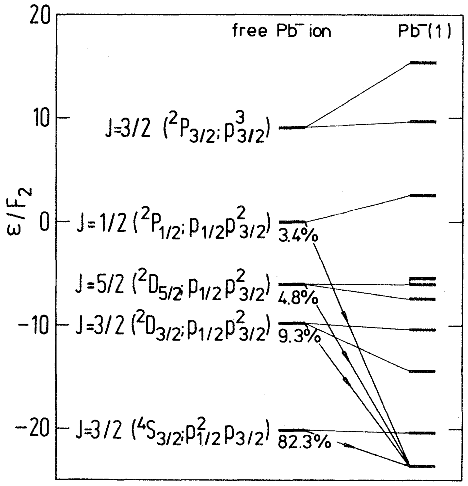

FIG. 4. Energy level diagram of the free Pb^- ion (left) compared with the one of the Pb^- (1) defect in KCl:PbCl$_2$. Both are calculated with $\xi/F_2=8.5$ (see Fig. 6). The crystal-field parameters for Pb^- (1) are given in Table II. The arrows indicate the admixture of the free-ion states into the Pb^- (1) ground state caused by the strong crystal field. The Slater-Condon parameter F_0 was not taken into account in this figure.

in which $\vec{r}=(r,\theta,\phi)$ are the polar coordinates of the electron. Only the $l=2$ terms in this sum have nonzero matrix elements between the *p* orbitals (5). By a suitable choice of reference frame, and because v_c is a real function, one can simplify to

$$-e v_c(\theta,\phi) = \mathfrak{D}(\cos^2\theta-\tfrac{1}{3}) + \mathcal{E}\sin^2\theta(\cos^2\phi-\sin^2\phi)\ , \tag{8a}$$

with

$$\mathfrak{D}=(45/16\pi)^{1/2}A_{20}\langle r^2\rangle\ ,$$
$$\mathcal{E}=(15/8\pi)^{1/2}A_{22}\langle r^2\rangle\ , \tag{8b}$$

where $\langle r^2\rangle$ has been averaged between the common $R_{6p}(r)$ radial function.

In the cases where the $S=\frac{3}{2}$ formalism can be applied, i.e., when the matrix elements of the crystal field v_c between different levels of the free ion are much smaller than the corresponding energy splittings, the parameters $\mathfrak{D}$ and $\mathcal{E}$ are proportional to *D* and *E* in spin Hamiltonian (2). A detailed inspection shows that the signs of *D* and *E* are always opposite to those of $\mathfrak{D}$ and $\mathcal{E}$, respectively. Useful selection rules for the matrix elements

$$\langle LSM_LM_S|V_c|L'S'M_L'M_S'\rangle$$

are the following:

$$\Delta S = S-S' = \Delta M_S = M_S - M_S' = 0\ ,$$

and

$$\Delta M_L = M_L - M_L' = -2, 0, \text{ or } +2\ .$$

Nonzero matrix elements occur only between the ${}^2P$ and the ${}^2D$ manifolds, and for each M_S value the following off-diagonal matrix elements are presented in Table II.

The eigenstates of $\mathcal{H}(\text{Pb}^-)$ are now readily obtained by diagonalization of the 20×20 matrix. Closer inspection shows that it can be separated into two 10×10 matrices which are related to each other by time-reversal symmetry. For nonzero values of the crystal-field parameters $\mathfrak{D}$ and $\mathcal{E}$, a Kramers doublet forms the lowest level. If one of the ground states is obtained from diagonalization of one of the 10×10 matrices as

$$|g\rangle = \sum_{L,S}\sum_{M_L,M_S} C_{LSM_LM_S}|LSM_LM_S\rangle\ ,$$

where the real coefficients $C_{LSM_LM_S}$ are zero unless $M_J=M_L+M_S=-\frac{3}{2}, \frac{1}{2}$, or $\frac{5}{2}$, then the second one is obtained by time conjugation[26]:

$$|\bar{g}\rangle = \sum_{L,S}\sum_{M_L,M_S} C_{LSM_LM_S}(-1)^{L-M_L+S-M_S} \times |L,S,-M_L,-M_S\rangle$$

TABLE II. Off-diagonal matrix elements of the model Hamiltonian $\mathcal{H}$ [Eqs. (6)–(8)] for each M_S value.

	$\lvert{}^2D,-2,M_S\rangle$	$\lvert{}^2D,-1,M_S\rangle$	$\lvert{}^2D,0,M_S\rangle$	$\lvert{}^2D,1,M_S\rangle$	$\lvert{}^2D,2,M_S\rangle$
$\langle{}^2P,-1,M_S\rvert$	0	$\frac{2}{5}\mathfrak{D}$	0	$\frac{2}{5}\mathfrak{D}$	0
$\langle{}^2P,0,M_S\rvert$	$-\sqrt{8}\mathcal{E}/5$	0	0	0	$\sqrt{8}\mathcal{E}/5$
$\langle{}^2P,1,M_S\rvert$	0	$-\frac{2}{5}\mathfrak{D}$	0	$-\frac{2}{5}\mathfrak{D}$	0

if the usual phase relation between the LS states is chosen. The ground doublet is now identified with the states of the effective $S=\frac{1}{2}$ spin Hamiltonian (3). The g^{eff} parameters are calculated from the matrix elements of the Zeeman Hamiltonian

$$\mathcal{H}_Z=\sum_i \mu_B\vec{\mathrm{H}}\cdot(\vec{\mathrm{l}}_i+2\vec{\mathrm{s}}_i)=\mu_B\vec{\mathrm{H}}\cdot(\vec{\mathrm{L}}+2\vec{\mathrm{S}})$$

within the ground doublet. The operators $\vec{\mathrm{L}}$ and $\vec{\mathrm{S}}$ do not possess matrix elements between different LS manifolds and within a manifold the matrix elements are easily calculated.

In order to eliminate redundant calculations only the range of $\mathfrak{D}$ and $\mathcal{E}$ values limited by

$$\mathfrak{D}\leqslant 0,\quad \mathfrak{D}\leqslant\mathcal{E}\leqslant 0 \tag{9}$$

must be considered. Indeed, permutation of the reference axes transforms the crystal-field parameters according to

$$\mathfrak{D}(\vec{\mathrm{z}},\vec{\mathrm{x}},\vec{\mathrm{y}})=-\tfrac{1}{2}\mathfrak{D}(\vec{\mathrm{x}},\vec{\mathrm{y}},\vec{\mathrm{z}})+\tfrac{3}{2}\mathcal{E}(\vec{\mathrm{x}},\vec{\mathrm{y}},\vec{\mathrm{z}})\ ,$$

$$\mathcal{E}(\vec{\mathrm{z}},\vec{\mathrm{x}},\vec{\mathrm{y}})=-\tfrac{1}{2}\mathfrak{D}(\vec{\mathrm{x}},\vec{\mathrm{y}},\vec{\mathrm{z}})-\tfrac{1}{2}\mathcal{E}(\vec{\mathrm{x}},\vec{\mathrm{y}},\vec{\mathrm{z}})\ ,$$

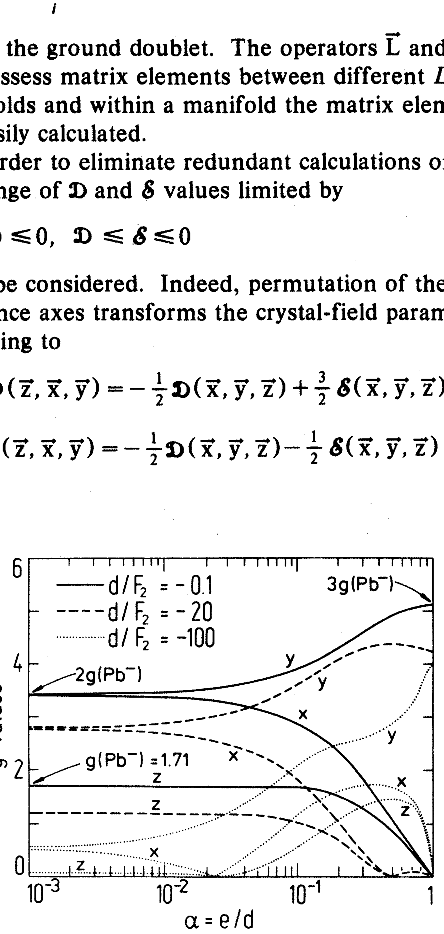

FIG. 5. The calculated g^{eff} components for Pb^- in an orthorhombic crystal field as a function of the crystal-field ratio $\alpha=\mathcal{E}/\mathfrak{D}$ for three values of $\mathfrak{D}/F_2$, the ratio of the dominant crystal-field term $\mathfrak{D}$ to the Slater-Condon parameter F_2. In the calculation the spin-orbit-coupling parameter was taken as $\xi=8.5\ F_2$ (see Fig. 6 and Table IV).

which yields

$$\alpha(\vec{\mathrm{z}},\vec{\mathrm{x}},\vec{\mathrm{y}})=\frac{\mathcal{E}}{\mathfrak{D}}=\frac{1+\alpha(\vec{\mathrm{x}},\vec{\mathrm{y}},\vec{\mathrm{z}})}{1-3\alpha(\vec{\mathrm{x}},\vec{\mathrm{y}},\vec{\mathrm{z}})}\ ,$$

and, in a second case according to

$$\mathfrak{D}(\vec{\mathrm{y}},\vec{\mathrm{z}},\vec{\mathrm{x}})=-\tfrac{1}{2}\mathfrak{D}(\vec{\mathrm{x}},\vec{\mathrm{y}},\vec{\mathrm{z}})-\tfrac{3}{2}\mathcal{E}(\vec{\mathrm{x}},\vec{\mathrm{y}},\vec{\mathrm{z}})\ ,$$

$$\mathcal{E}(\vec{\mathrm{y}},\vec{\mathrm{z}},\vec{\mathrm{x}})=\tfrac{1}{2}\mathfrak{D}(\vec{\mathrm{x}},\vec{\mathrm{y}},\vec{\mathrm{z}})-\tfrac{1}{2}\mathcal{E}(\vec{\mathrm{x}},\vec{\mathrm{y}},\vec{\mathrm{z}})\ ,$$

and

$$\alpha(\vec{\mathrm{y}},\vec{\mathrm{z}},\vec{\mathrm{x}})=\frac{1-\alpha(\vec{\mathrm{x}},\vec{\mathrm{y}},\vec{\mathrm{z}})}{1-3\alpha(x,y,z)}\ .$$

Moreover, it is seen that an interchange of the $\vec{\mathrm{x}}$ and $\vec{\mathrm{y}}$ directions leaves $\mathfrak{D}$ unchanged and reverses the sign of $\mathcal{E}$, and thus also of α. By suitable choice of the reference axis one can describe any crystal field v_c [Eqs. (8)] using $\mathfrak{D}$ and $\mathcal{E}$ parameters within the range given above [Eqs. (9)]. Exactly the same transformation properties are found for the spin-Hamiltonian parameters D and E [see Eq. (2)].

In Fig. 5 the g^{eff} parameters of the Pb^- ion, calculated for three different values of $\mathfrak{D}/F_2$, are plotted as a function of the ratio $\alpha=\mathcal{E}/\mathfrak{D}$. The ratio $\xi/F_2=8.5$ which was used for Pb^- is discussed below. For a weak crystal field $\mathfrak{D}$ ($\mathfrak{D}/F_2<<1$) the g^{eff} parameters of the $S=\frac{3}{2}$ formalism [Eqs. (4)] are recovered with an isotropic g factor $g\ (\mathrm{Pb}^-)=1.71$ of the free Pb^- ion. For values of $\mathfrak{D}$ and $\mathcal{E}$ comparable to the free-ion energy splittings, large deviations are found from the $S=\frac{3}{2}$ relations [Eqs. (4)]. A very close fit of the experimental g^{eff} parameters is now possible for each of the Pb^- defects.

2. *Fit of the experimental g^{eff} parameters*

A variation of the model parameters ξ/F_2, $\mathfrak{D}/F_2$, and $\alpha=\mathcal{E}/\mathfrak{D}$, allows a fit of the experimental g^{eff} values for each of the Pb^- defects in KCl. The best fits for Pb^- (1), Pb^- (2), and Pb^- (4) were obtained by a minimalization of the function

$$\Phi=\sum_{i=x,y,z}\left[\frac{g_i^{\mathrm{calc}}-g_i^{\mathrm{expt}}}{g_i^{\mathrm{expt}}}\right]^2\ ,$$

the sum of the squares of the relative errors on the g^{eff} parameters. For values of ξ/F_2 between 1 and 20 the function Φ was minimized with respect to $\mathfrak{D}/F_2$ and $\alpha=\mathcal{E}/\mathfrak{D}$. The minimum value Φ_{min} is used to calculate the variance Φ'_{min} of the g^{eff} parameters,

$$\Phi'_{\text{min}}=(\Phi_{\text{min}}/3)^{1/2}\ , \tag{10}$$

which is a measure for the average relative difference between the experimental and theoretical g^{eff} values. This minimal value of the variance is shown in Fig. 6 as a function of ξ/F_2. The best fits of the g^{eff} values are obtained for values around $\xi/F_2=8.5$, and it is comforting to see that the minima of the Φ_{min} curves for the defects lie very near to each other. Later in this section this value of $\xi/F_2=8.5$ is shown to be close to what is obtained from an extrapolation of the ξ and F_2 values using the atomic data from the isoelectronic series Rn^{3+}, At^{2+}, Po^{+}, and Bi^{0}.

The best fits of the g^{eff} parameters of Pb^- (1), Pb^- (2), and Pb^- (4) obtained for $\xi/F_2=8.5$ are listed in Table III, together with the corresponding crystal-field parameters. The z axis is chosen along the direction with lowest g value. This corresponds to a dominant negative $\mathfrak{D}$ component of the crystal field along this axis. We have always chosen the y axis along the principal direction of the defect which is parallel to $\langle 100\rangle$. For this reason we have to use both positive and negative values of α to list the crystal-field parameters calculated for the Pb^- defects (Table III).

A slightly different fitting procedure had to be applied for Pb^- (3) because only two independent g^{eff} values, i.e., g_y^{eff} and

$$g^{\text{eff}}(\theta=60^\circ,\phi=54.7^\circ)=\{\tfrac{1}{2}(g_y^{\text{eff}})^2+\tfrac{1}{4}[(g_x^{\text{eff}})^2+(g_z^{\text{eff}})^2]\}^{1/2}$$

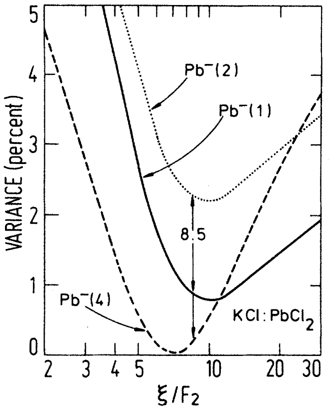

FIG. 6. The variance Φ'_{min} of the g^{eff} parameters [see Eq. (10)] which is obtained from a minimalization procedure with respect to the crystal-field parameters $\mathfrak{D}/F_2$ and $\alpha=\mathcal{E}/\mathfrak{D}$, is shown as a function of the ratio of the atomic parameters ξ/F_2. The value $\xi/F_2=8.5$, which was chosen for fitting the g^{eff} parameters of the Pb^- defects, is indicated by vertical arrows.

could be measured. The ratio $\xi/F_2=8.5$ was not varied. The crystal-field parameters $\mathfrak{D}$ and $\mathcal{E}$ were determined in such a way that the theoretical g^{eff} values exactly reproduce both the experimental g_y^{eff} and g^{eff} ($\theta=60^\circ$, $\phi=54.7^\circ$). This yields the $\mathfrak{D}$ and $\mathcal{E}$ parameters as well as the theoretical g_x^{eff} and g_y^{eff} values (see Table III).

The energy-level diagram of the Pb^- (1) defect is shown in Fig. 4 together with that of the hypothetical free Pb^- ion. The parameters given in Table III are adopted. It is observed that the energy shifts and splittings resulting from the crystal field are compar-

TABLE III. Best fit of the g_i^{eff} parameters of the Pb^- defects in KCl, obtained for the ratio $\xi/F_2=8.5$ (see text). The calculated g_i^{eff} values are compared to the experimental ones and the crystal-field parameters $\mathfrak{D}/F_2$ and $\alpha=\mathcal{E}/\mathfrak{D}$ are listed; F_2 is estimated to be $\approx 800\ \text{cm}^{-1}$.

		g_x^{eff} $\langle 110\rangle$	g_y^{eff} $\langle 100\rangle$	g_z^{eff} $\langle 110\rangle$	$\mathfrak{D}/F_2$	$\alpha=\mathcal{E}/\mathfrak{D}$
Pb^- (1)	expt.	3.555	1.151	0.6857		
	theor.	3.526	1.141	0.6925	−26.0	−0.124
Pb^- (2)	expt.	1.114	3.668	0.6595		
	theor.	1.090	3.590	0.6758	−25.7	0.132
Pb^- (3)	expt.	. . . [a]	4.033	. . . [a]		
	theor.[a]	1.171	4.033	0.7922	−19.6	0.182
Pb^- (4)	expt.	3.792	1.546	0.9458		
	theor.	3.785	1.543	0.9477	−20.1	−0.130

[a] The g_x^{eff} and g_z^{eff} values could not be experimentally determined. The crystal-field parameters are determined in such a way that the experimental values of g_y^{eff} and g^{eff} ($\theta=60^\circ$, $\phi=54.7^\circ$) $=2.938$ (see Table I) are exactly reproduced by the theory.

able in magnitude to the free-ion level splittings. Arrows indicate sizable admixture of excited states of the free Pb^- ion in the ground doublet of the Pb^- (1) defect. The amount of admixture is given in percentage for each contributing free-ion level. It is seen to be rather important (a total of 17.5%), and it has quite an influence on the ground-state g parameters because different J values are mixed in by the crystal field. These observations justify our approach of a full diagonalization of the energy matrix, which is not easy to replace by an approximation scheme.

3. Estimation of the atomic parameters of Pb^-

Since the free Pb^- ion may not be a stable species, no atomic data are directly available. A compilation of data of ions with a $6p^3$ configuration, Rn^{3+}, At^{2+}, Po^+, and Bi^0, are given in Table IV. Optical data are available only for Bi^0, Pb^+ ($6p^1$), and Pb^0 ($6p^2$). From relativistic Hartree-Fock calculations, values are available for the other ions.[27,28] The spin-orbit parameters are quite reliable although they are believed to be slightly overestimated. The Slater-Condon parameter is also overestimated by (20–30)%. This observation follows from a comparison of the data in the first and second columns of Table IV for the Bi^0 and Pb^0 atoms.

The calculated values of ξ and F_2 possess a nearly linear behavior as a function of the atomic number in the isoelectronic series of Pb^-. By linear extrapolation, using the theoretical values for Po^+ and Bi^0, one obtains "theoretical" values of ξ and F_2 for the Pb^- ion. The latter are reduced by the same percentage as found for Bi^0 (5% for ξ, 24% for F_2) in order to obtain the following estimate of the atomic parameters for Pb^-:

$$\xi \cong 6100\ \text{cm}^{-1}, \quad F_2 \cong 800\ \text{cm}^{-1} \ .$$

The resulting ratio ξ/F_2 is close to the ratio 8.5 obtained from the best fits of the g^{eff} parameters of Pb^- in KCl. This supports the validity of our analysis. We note in passing that for Sn^- the values $\xi \cong 1500$ cm^{-1} and $F_2 \cong 730\ \text{cm}^{-1}$ were estimated.[17]

The parameters ξ and F_2 are expected to decrease through the series Pb^+, Pb^0, and Pb^-, because the atomic orbitals tend to compress when the net charge of the ion increases towards positive values. This is in agreement with the values shown in Table IV and those given above for the Pb^- ion. The extrapolation of ξ and F_2 is a rather rough procedure. Moreover, it is not known for certain whether or not Pb^- is a stable ion in the free state. A relativistic restricted Hartree-Fock calculation[27] yields a stable Pb^{x-} ion for values of x up to ≈ 0.95. An unrestricted calculation could conceivably yield a stable ion for $x=1$. It may be that the Pb^- ion in KCl is stable only because of the crystalline environment, and this can have an influence on the magnitude of the atomic parameters. Therefore, the value $\xi/F_2 = 8.5$ is considered to be the most reliable one, because it is derived from experimental data.

TABLE IV. Atomic parameters derived from optical data (ξ^{opt} and F_2^{opt}) or from relativistic Hartree-Fock calculations (ξ^{RHF} and F_2^{RHF}), given in wave numbers.

Ion	ξ^{opt}	F_2^{opt}	ξ^{RHF}	F_2^{RHF}
Rn^{3+}			25 000[c]	
At^{2+}			19 600[c]	1790[c]
Po^+			14 800[c]	1590[c]
Bi^0	10 100[a]	990[a]	10 600[c]	1320[c]
Pb^0	7294[a]	921.5[a]	8070[d]	1200[c]
Pb^+	9400[b]	. . .		

[a] Reference 25.

[b] Determined from $\xi^{\text{opt}} = \frac{2}{3}\Delta$, where Δ is the experimental energy splitting between the $6p_{1/2}$ and the $6p_{3/2}$ states of the ground configuration of Pb^+.

[c] J. Andriessen (private communication).

[d] From Ref. 28.

D. Comparison of the Pb^- and Sn^- crystal fields

In Ref. 17 the axial crystal-field parameters of the spin Hamiltonian (2) was very roughly estimated to be $D \approx 27\ \text{cm}^{-1}$ for the anisotropic Sn^- defects in KCl:Sn^{2+}. The corresponding crystal-field splitting $2D \approx 54\ \text{cm}^{-1}$ is very small compared to the ground-state splitting of the various Pb^- defects which is calculated to be $\approx 2500\ \text{cm}^{-1}$ (see Fig. 4). The question arises whether the crystal fields that the Pb^- undergo are really about two orders of magnitude larger than in the case of Sn^-. The answer is no: the *effect* of the crystal potential is felt more strongly by Pb^- because of the appreciable orbital angular momentum mixing in the ground state compared to Sn^- and because Pb^- probably possesses a somewhat larger $\langle r^2 \rangle$ value than Sn^-.

In order to demonstrate this the procedure of Sec. IVC was used and the ground-state splittings of the Sn^- and Pb^- ions were calculated in an axial field of the type (8) with $\mathfrak{D} = -10^4\ \text{cm}^{-1}$, i.e., a $\mathfrak{D}$ value comparable to those found for the Pb^- defects (see Table III). The calculations yield a splitting of $\sim 13\ \text{cm}^{-1}$ for Sn^- and of $\sim 880\ \text{cm}^{-1}$ for Pb^-. This separation is quite sensitive to small changes in the values of the atomic parameters, going with the third power of ξ/F_2 in the case of Sn^-. However, it is abundantly clear that for comparable crystal-field potentials the Sn^- and Pb^- ground-state splittings differ from each other by nearly two orders of magnitude. Similar results were found for pure orthorhombic fields ($\mathfrak{D}=0$, $\mathcal{E}\neq 0$).

E. Possibility of Jahn-Teller distortions in the case of Pb^- centers

The possible structures for the various Pb^- centers will be discussed in Sec. VI but because of the sizable orbital angular momentum presence in the fourfold-degenerate ground state of the free Pb^- ion, it seems quite possible that in at least one of these centers the Pb^- occupies an unperturbed octahedral anion site having undergone a mixture of E_g- and T_{2g}-type Jahn-Teller (JT) distortions. The latter are possible JT deformations because[29] $\Gamma_8\times\Gamma_8$ contains E_g and T_{2g}; Γ_8 is the Pb^- ground state in an octahedral environment.

A rough estimate of the JT energy is the difference of the ground-state energies of the free Pb^- ion and of the Pb^- (1) defect and from Fig. 7 one deduces $E_{JT}(Pb^-)\cong 2500\ cm^{-1}$. This value is many times a typical phonon frequency ($\sim 200\ cm^{-1}$) and a static JT effect is indeed expected to occur.

The foregoing conclusion hinges on whether or not a distortion of reasonable size, 10% say, does indeed result in a crystal-field strength $\mathfrak{D}\cong -2\times 10^4\ cm^{-1}$ (see Table III), and consequently in a E_{JT} (Pb^-) $\cong 2500\ cm^{-1}$. To this end the $\mathfrak{D}$ and $\mathcal{E}$ parameters resulting from the displacement of only the nearest-neighbor K^+ ions are calculated in a simple point-ion approximation:

$$\mathfrak{D}=-9e^2(\tfrac{3}{2}q_E+q_T)\langle r^2\rangle/R^4\ ,$$

$$\mathcal{E}=-3e^2(\tfrac{9}{2}q_E-q_T)\langle r^2\rangle/R^4\ ,$$

in which $R=5.95$ a.u. is the Pb^-—K^+ distance, and q_E and q_T are the distortion coordinates. In a pure E_g mode the K^+ ions in the (x,z) plane [see Fig. 18(a)] are displaced by q_E towards the Pb^- ion, while the two K^+ ions on the z axis are displaced outwards by $2q_E$. In a pure T_{2g} distortion the four K^+ ions are displaced by q_T perpendicular to the line connecting the Pb^- to the K^+ ion. For this calculation one needs the $\langle r^2\rangle$ value for the $6p$ orbital of Pb^-. For the Tl^0 $6p$ electron $\langle r^2\rangle$ was calculated to be[19] 12 a.u. The Pb^- value could be somewhat larger. Using $\langle r^2\rangle=12$ a.u. as a lower bound for Pb^-, we obtain the Pb^- (2) parameters $\mathfrak{D}=-2\times 10^4\ cm^{-1}$ and $\alpha=0.13$ for a combined E_g and T_{2g} distortion $q_E=0.041R$ and $q_T=0.115R$. It is concluded that the size of the observed crystal-field strength (Table III) can easily be caused by a JT deformation and that E_{JT} (Pb^-) $\sim 10^3$ cm^{-1} is a reasonable magnitude for the JT energy.

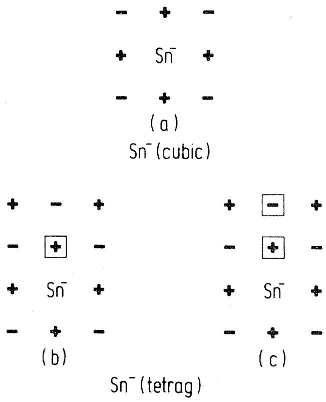

FIG. 7. (a) Schematic two-dimensional model in a {100} plane of the Sn^- (cubic) center in KCl:Sn^{2+}; (b), (c) two most probable models of the Sn^- (tetrag) center in KCl:Sn^{2+} (from Ref. 17).

If E_{JT} (Pb^-) $\cong 2500\ cm^{-1}$, then based on the calculation presented in the preceding subsection we estimate for a Sn^- on an unperturbed anion site in KCl that E_{JT} (Sn^-) $\cong 30\ cm^{-1}$. This is far too small to result in a static JT distortion and a motionally averaged ESR spectrum is expected even at very low temperatures. An isotropic Sn^- ESR spectrum was indeed observed[17] in KCl:Sn^{2+} at temperatures as low as 2 K and it was attributed to a Sn^- on an octahedral anion site [see Fig. 7(a)]. The viewpoint that this Sn^- (cubic) center was a dynamic JT system was not stressed in Ref. 17, but that it may be such a system is underscored by the observation that the Sn^- (cubic) ESR line is exceedingly sensitive to external uniaxial stress: in a preliminary experiment we have observed that a weak stress applied at liquid-He temperatures rapidly splits and broadens the ESR line. If the Sn^- were pure $^4S_{3/2}$ no such strong effects would be expected.

One might extend this type of reasoning to the Sn^- (tetrag) center observed in KCl:Sn^{2+}. In this defect of tetragonal symmetry around $z\parallel\langle 100\rangle$ a substitutional Sn^- on an anion site is perturbed by a nearest-neighbor positive-ion vacancy or a divacancy [Figs. 7(b) and 7(c)]. One can easily imagine that such a structure also occurs for a Pb^- center. In a strong—crystal-field picture one can argue that the p_z orbital is repelled by the negative charge of the positive-ion vacancy, leaving the three electrons in a degenerate $\{p_x,p_y\}$ pair in a {100} plane perpendicular to the $z\parallel\langle 100\rangle$ direction. This last degeneracy will be lifted by a JT distortion in the {100} plane. If the E_{JT} is sufficiently large a static JT effect will result and an orthorhombic ESR spectrum will be observed in spite of the fact that such a Pb^--center model, at a first glance, seems to possess tetragonal symmetry around $\langle 100\rangle$.

V. PRODUCTION, THERMAL, AND PHOTOCHEMICAL PROPERTIES OF THE Pb^- DEFECTS

In Sec. IV it was shown that the basic entity underlying the four ESR spectra must be in each case a

Pb^- ion occupying a negative ion site. The four centers differ among each other by the magnitude of the crystal-field parameters, i.e., by the nature and number (if any) of the perturbing entities in the immediate vicinity of the Pb^- ion. In the present section, results are presented of various experiments which were performed with the aim of better understanding the production and precise structure of the various Pb^- defects. These experiments deal primarily with production by x irradiation, thermal annealing, and optical excitation. In all the experiments the changes in the Pb^--center concentrations were monitored by measuring the intensities of corresponding ESR transitions under the same recording conditions and with the static magnetic field along $\langle 100 \rangle$. In monitoring the concentration changes the $\theta = 90°$, $\phi = 90°$ transition was used for Pb^- (1) and Pb^- (3) and the $\theta = 45°$, $\phi = 0°$ transition for Pb^- (2) and Pb^- (4).

It was noted in Sec. IV in connection with the ESR parameters, the g values in particular, that the Pb^- centers should be grouped into the Pb^- (I)-type centers Pb^- (1) and Pb^- (4), and the Pb^- (II)-type centers Pb^- (2) and Pb^- (3). It will become clear in the present section that this classification also reflects on many of their production, thermal, and photochemical properties.

A. Production and thermal properties

No Pb^- ESR spectra are observed in $KCl{:}Pb^{2+}$ either after x irradiation at 77 K or after a subsequent warmup to any temperature. The same behavior is observed for x irradiations at temperatures approaching 220 K, but above this temperature it becomes possible to produce all four Pb^- defects. Figure 8 shows the intensities of these centers after 20 min of x irradiation at successive temperatures above 220 K. Before each x irradiation the crystal was restored to its initial state by heating it to about 500 °C. By this treatment all radiation-produced defects are eliminated. From Fig. 8 it is clear that for all Pb^- centers maximum production is attained in the temperature interval 250 to 280 K. The weak Pb^- (3) and Pb^- (4) ESR signals decrease below the detection limit for x irradiation above 280 K.

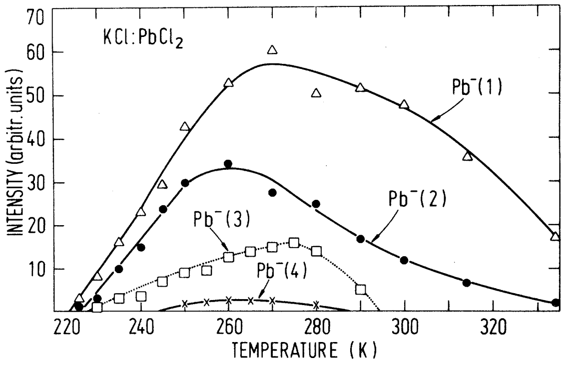

FIG. 8. Intensities of the four Pb^- centers in $KCl{:}PbCl_2$ obtained by x irradiations lasting 20 min at successive temperatures above 220 K. Before each x irradiation the sample was heated to about 500 °C in order to destroy all radiation-produced defects.

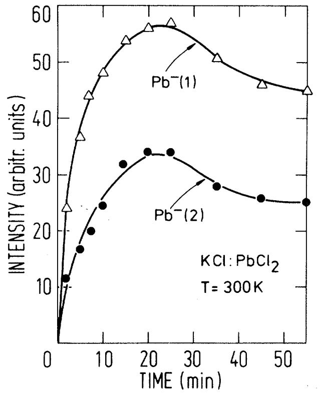

FIG. 9. Production of the Pb^- (1) and Pb^- (2) defects in $KCl{:}PbCl_2$ as a function of x-irradiation time at room temperature. A similar behavior is observed at lower irradiation temperatures.

The production of Pb^- (1) and Pb^- (2) centers as a function of x-irradiation time at RT is presented in Fig. 9. Both Pb^- defects reach a maximum after about 25 min for our particular experimental setup. The behavior at lower irradiation temperatures is similar, and this is also true for the Pb^- (3) and Pb^- (4) centers.

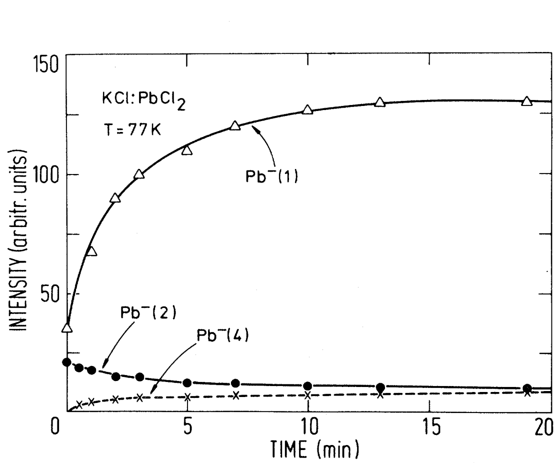

FIG. 10. Production of Pb^- centers in $KCl{:}PbCl_2$ as a function of x-irradiation time at 77 K in a sample which had first been x irradiated for 10 min at room temperature.

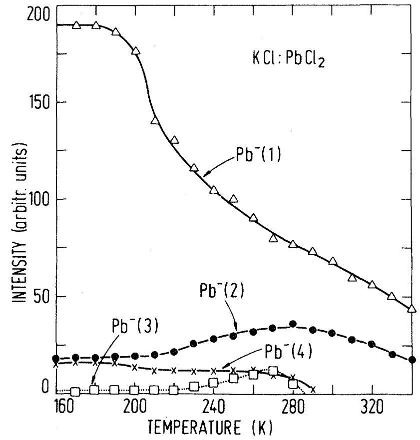

FIG. 11. Pulse-anneal results for a KCl:PbCl$_2$ sample which had first been subjected to a double x irradiation: 10 min at room temperature followed by 10 min at 77 K (see Fig. 10).

It was found that a higher concentration of Pb$^-$ (I)-type centers could be obtained by first x irradiating the KCl:Pb^{2+} sample at RT for 5–10 min, followed by an x irradiation of similar duration at 77 K. The change in the Pb$^-$-center concentrations by the second part of the treatment is shown in Fig. 10: Pb$^-$ (4) is produced in small quantities and Pb$^-$ (1) increases by a factor of 3; the Pb$^-$ (2) concentration decreases somewhat under this treatment.

Pulse-anneal experiments were performed on samples of KCl:Pb^{2+} which had been x irradiated for 10 min at RT and at 77 K. The results are presented in Fig. 11. Around 210 K a strong decrease in the concentration of the Pb$^-$ (I)-type defects is observed. This decrease coincides with the known Cl$_2$$^-$ V_K-center decay temperature.[30] It is concluded that part of the Pb$^-$ (I) defects are destroyed by trapping a mobile V_K-center hole thus forming what could be designated as a Pb^0 (I)-type center. The concentration of the two Pb$^-$ (II)-type centers shows an increase in the range 220 to 260 K. Whether or not this increase is correlated with the ongoing slower Pb$^-$ (I) decay could not be ascertained. Pb$^-$ (3) and Pb$^-$ (4) both disappear around 280 K.

In order to study the decay of the Pb$^-$ (1) and Pb$^-$ (2) centers another pulse-anneal experiment was performed on a KCl:Pb^{2+} sample x irradiated for 20 min at 260 K. The results are presented in Fig. 12: Around 270 K a small Pb$^-$ (2) increase is observed which appears to coincide with a much larger decay of Pb$^-$ (1). Above 300 K both centers decay and above 400 K Pb$^-$ ESR absorptions are no longer observed.

B. Behavior of the Pb$^-$ centers under optical F-center excitation

An F center is an electron trapped at an anion vacancy. Optical excitation in the F band ($\lambda = 539$ nm) at low temperatures (~ 15 K) produces mobile electrons in the lattice but the anion vacancies remain fixed. Only the mobile electrons can be retrapped at other existing electron-trap centers under a low-temperature optical F-center excitation.

The results of such an experiment are presented in Fig. 13 for a KCl:Pb^{2+} sample which had been x irradiated at 260 K for 20 min (see Fig. 8). The optical F-center bleach at 15 K results in a sizable increase of the Pb$^-$ (I)-type concentration but little change in the intensity of the Pb$^-$ (II)-type centers is observed. If the crystal is brought to RT after a 20-min x irradiation at 260 K, the effect of an F-band excitation at 15 K on the Pb$^-$ (1) concentration is even stronger: In Fig. 14, a tripling of the Pb$^-$ (1) intensity is observed.

Both experiments strongly point to the existence of electron-trap precursor centers for the two Pb$^-$ (I)-type defects. Such precursor centers will be called Pb^0 (I)-type centers. No precursor centers seem to exist for the Pb$^-$ (II) defects. Their small decrease in

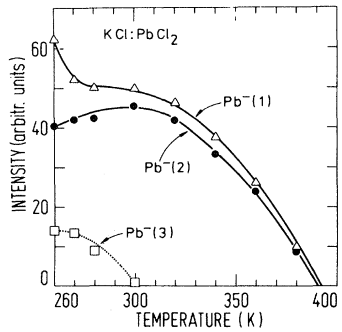

FIG. 12. Pulse-anneal results for a KCl:PbCl$_2$ sample which had been x irradiated for 20 min at 250 K (see Fig. 8).

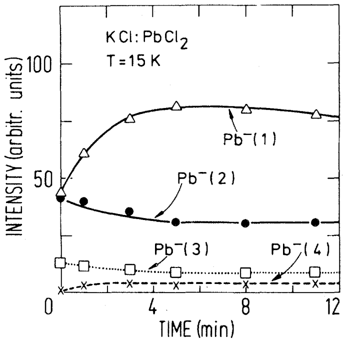

FIG. 13. Effect on the concentrations of the Pb$^-$ centers of an optical F-center excitation at 15 K. The sample had first been x irradiated for 20 min at 260 K (see Fig. 8).

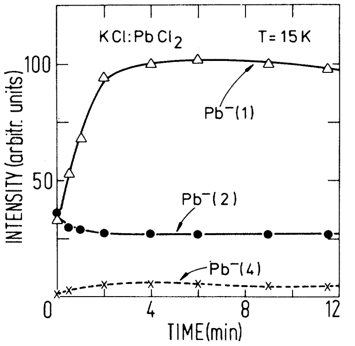

FIG. 14. Effect of an optical *F*-center excitation at 15 K on the Pb^--center concentrations. The sample had first been x irradiated for 20 min at 260 K (see Fig. 8) followed by a warmup to room temperature for another 20 min.

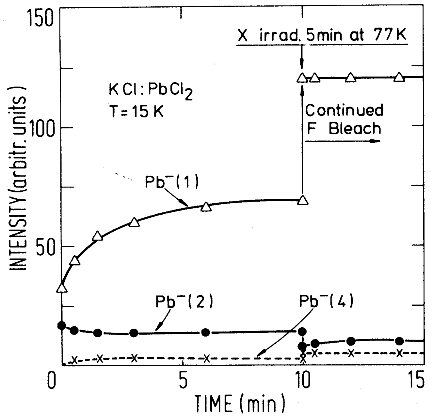

FIG. 15. Behavior of the Pb^--center concentrations under optical *F*-center excitation at 15 K in a sample which had first been x irradiated for 10 min at room temperature. After 10 min of optical excitation the sample was submitted to a 5-min x irradiation at 77 K after which the *F* bleach at 15 K was continued.

concentration under optical *F*-center excitation could indicate either the occurrence of a low—cross-section electron-trapping process leading to the production of some Pb^{2-} (II)-type centers, or direct optical excitation into an optical Pb^- (II) absorption band which would happen to coincide with the *F*-center absorption band.

These results obtained from *F*-band excitation experiments at low temperatures lead to a likely explanation for the mechanism by which high concentrations of Pb^- (1) centers are produced during an x irradiation at 77 K subsequent to an x irradiation at RT (see Fig. 10). The RT irradiation produces a large amount of Pb^0 (1) precursor centers and the 77-K irradiation produces mobile electrons which are attracted to and trapped by the Pb^0 (1) precursors to produce Pb^- (1). It may be emphasized here in passing that no such Pb^0 (1) precursors are produced by a simple x irradiation at 77 K because no Pb^- centers are observed after a subsequent optical *F*-center excitation at 15 K.

Even taking into account the experimental errors it is clear that the amount of Pb^- (1) produced by the double x irradiation at RT and at 77 K (Fig. 10) is higher than the amount produced by a low-temperature optical *F*-center excitation (Fig. 13). This is further illustrated by the following experiment, the results of which are presented in Fig. 15: A $KCl:Pb^{2+}$ sample was x irradiated for 10 min at RT and then optically excited in the *F* band at 15 K so as to achieve saturation (a doubling) in the production of Pb^- (1) centers. Subsequently, the sample was x irradiated for 5 min at 77 K leading to a substantial increase in the Pb^- (1) concentration. A further optical *F*-center excitation had no effect on the Pb^- (1) intensity, pointing to the fact that all Pb^0 (1) precursor centers had been used up. One possible explanation for the lower Pb^- (1) center yield under *F*-center excitation may be that, after 10 min of optical bleaching, a balance is achieved between the production of Pb^- (1) through electron trapping by the Pb^0 (1) precursor on the one hand and a destruction of Pb^- (1) centers, on the other hand, by direct optical excitation into a Pb^- (1) absorption band which would happen to be close to the *F* band. This, however, needs further study.

C. Behavior of the Pb^- centers under optical V_K-center excitation

Similar experiments were performed by optical excitation of the V_K-center band ($\lambda = 365$ nm) in samples which had first been x irradiated at RT and at 77 K. The latter irradiation strongly increases the Pb^- (1)-center concentration (Fig. 10) and also produces

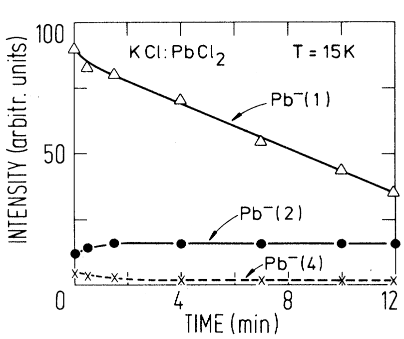

FIG. 16. Effect on the Pb^--center concentrations of an optical V_K-center excitation at 15 K using 343-nm light. The sample had first been x irradiated for 10 min at room temperature followed by an equally long x irradiation at 77 K (see Fig. 10).

a large amount of Cl_2^- V_K centers. Optical excitation of V_K centers results in the production of mobile positive holes in the lattice. As shown in Fig. 16 the Pb^- (1) center decreases strongly under such treatment while Pb^- (2) remains virtually untouched. This behavior parallels very much the one observed in Fig 11: The strong partial Pb^- (1) decay around 210 K was ascribed to trapping of holes from mobile V_K centers. If the destruction of Pb^- (1) is indeed caused by the trapping of a mobile hole, then Pb^0 (1) centers are produced. However, the possibility that Pb^- (1) decays because of a direct excitation into a Pb^- (1) optical absorption band which happen to be near the 365-nm region cannot be excluded without further investigation.

VI. MODELS FOR THE Pb^- CENTERS

In trying to establish models for the various Pb^- defects one can draw on the data presented in this paper and on the results obtained for the Sn^- defects in Ref. 17. In spite of all this extensive information, the task turns out to be a difficult one. Therefore, we will from the outset simplify this task by trying to find models for the dominant Pb^- (1) and Pb^- (2) defects only. We have remarked on several occasions that in many properties Pb^- (4) resembles Pb^- (1) [they were called Pb^- (I)-type centers] and similarly for Pb^- (3) and Pb^- (2) [the Pb^- (II)-type centers]. The Pb^- (3) and Pb^- (4) models are likely to represent variations (albeit complex) on a basic theme defined by the Pb^- (2) and Pb^- (1) models, respectively.

Because all four Pb^- defects possess orthorhombic symmetry, one can search for models in which a Pb^- on an anion site is, in general, perturbed by one or more defects in the immediate vicinity. On the one hand, it is unlikely that these perturbing entities are unintentional impurities: All four Pb^- centers occur in samples grown from very pure KCl (Br^- and Na^+ impurity content <10 ppm) in a chlorine atmosphere (very little oxygen content). On the other hand, it is abundantly clear from the results obtained in Sec. V that the Pb^- defects are created by treatments involving at least one x irradiation above 220 K. Because at and above this temperature positive- and negative-ion vacancies become mobile,[17,19,22–24] it is very likely that the perturbing defects are vacancies. These are the only perturbations that will be considered.

In the following the merits and deficiencies of two classes of Pb^--center models will be discussed: vacancy models and Jahn-Teller models. To be sure, both classes involve vacancies, but in the vacancy models the Pb^- orthorhombic symmetry is induced by one or more vacancies, whereas in the JT models the orthorhombic symmetry is induced by a static JT distortion of the Pb^- surroundings (see Sec. IV 3 E) and nearby vacancies merely exert an additional perturbation.

A. Vacancy models

As stated above in the class of vacancy models the possibility of a static JT distortion is ignored and it is assumed that the symmetry of the Pb^- defects is determined by the number and type of vacancies in the immediate vicinity of the substitutional Pb^-. This is in essence the procedure which was followed to find plausible models for the Sn^- defects.[17] In Sec. IV C it was established that the dominant crystal-field component $\mathfrak{D}$ was strongly attractive along $z \parallel \langle 110 \rangle$ and the proposed models should possess this property.

Figures 17(a)–17(e) present some possible defect configurations. Not surprisingly, they are similar to the ones proposed for the Sn^- (ortho) centers.[17] In Figs. 17(a) and 17(b) the negative ion vacancies will attract the unpaired electrons making that the dominant crystal-field term $\mathfrak{D}$ is along the $\langle 110 \rangle$ direction defined by the Pb^- and the vacancies. The model in

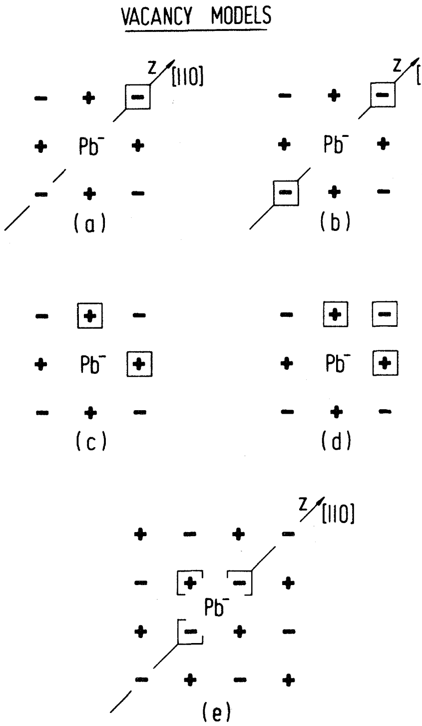

FIG. 17. Schematic two-dimensional representation in a {100} plane of a few simple "vacancy models" for the Pb^- centers. In the vacancy models the orthorhombic symmetry of the Pb^- centers is induced by the vacancies. Note the subtle differences between models (a) and (b) and those of (b) and (c) in Fig. 18.

Fig. 17(c) appears unstable because of the two cation vacancies repel each other. In fact the linear configuration along ⟨100⟩ in which the substitutional Pb^- is flanked by the two cation vacancies is more likely to possess the lower energy. In Fig. 17(d) this problem is alleviated somewhat because the additional anion vacancy can act as a glue between the two cation vacancies. It is not obvious for the latter two models what the direction of the dominant crystal-field term will be. Finally, Fig. 17(e) presents an electrically neutral model with Pb^- occupying a symmetric interstitial position in between the two anion vacancies.

It turns out to be quite difficult to associate any two of these models with Pb^- (1) and Pb^- (2). The results presented in Table III show that Pb^- (1) and Pb^- (2) possess virtually identical $\mathfrak{D}$ values but opposite $\alpha = \mathcal{E}/\mathfrak{D}$ values (i.e., the crystal field axes x and y are interchanged). It is not obvious which of the five possibilities shown in Fig. 17 generate comparable $\mathfrak{D}$ values. In particular, it seems impossible that models (a) and (b) in Fig. 17 yield the same d value or opposite α values. Without the help of detailed calculations it cannot be said for the other models whether or not the sign of α will change from one to the other. The optical, thermal, and production data of Sec. V are not very helpful either, primarily because the detailed production sequences and mechanisms are not very well known.[17] If we must make a choice, then the models of Figs. 17(a) and 17(e) are favored because they could conceivably possess a comparable $\mathfrak{D}$ value (two anion vacancies are involved in both cases) and the sign of $\alpha = \mathcal{E}/\mathfrak{D}$ could be different for the two. However, a more specific identification with Pb^- (1) and Pb^- (2) is not possible without further investigation.

Within the framework of the vacancy models, one glaring question remains unanswered: Why are no Pb^- defects formed analogous to the Sn^- (cubic) and Sn^- (tetrag) centers (Fig. 7) which are so easily and strongly produced in KCl:Sn^{2+}? One does not expect the properties of Sn^{2+} and Pb^{2+} impurities to be so drastically different from each other that those two types of Pb^- centers would not be formed at all.

B. Jahn-Teller models

The Jahn-Teller models offer a more fruitful base for discussion. In these models it is assumed that the neighborhood of the substitutional Pb^- undergoes a strong JT distortion and that vacancies, if present, merely exert an additional perturbation on the center. The likelihood for the occurrence of static JT distortions for Pb^- was discussed in Sec. IV E. A few possible simple structures all involving JT distortions are presented in Figs. 18(a)–18(d).

Figure 18(a) represents a Pb^- ion on an unperturbed anion site having undergone a mixture of E_g and T_{2g} distortions (only the displacements of the nearest neighbor K^+ ions in a {100} plane are indicated on this schematic figure). This model is structurally identical to the Sn^- (cubic) center shown in Fig. 7(a). A simple electrostatic consideration strongly suggests that the z axis of the center is oriented as shown in this figure.

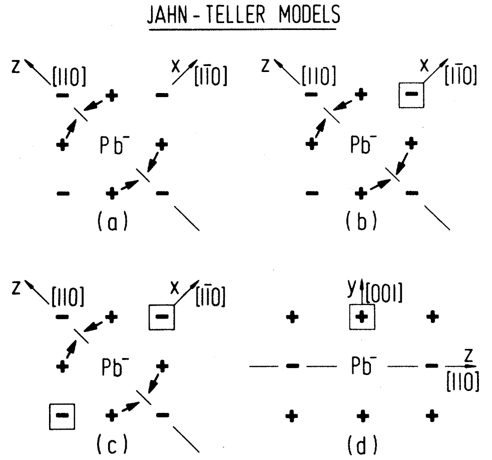

FIG. 18. Schematic two-dimensional representation of several "Jahn-Teller models" for the Pb^- centers. In these models the orthorhombic symmetry is induced by a JT deformation of the immediate surroundings, and the vacancies merely exert an additional perturbation. In model (d) (represented in a {110} plane) the perturbation could also be a divacancy as in Fig. 7(c). Note the difference of models (b) and (c) with those of Figs. 17(a) and 17(b).

In Figs. 18(b)–18(d) this basic structure is perturbed by vacancies but in all cases the JT distortion is assumed to be the strongest effect and the dominant crystal-field term $\mathfrak{D}$ remains oriented along $z \parallel [110]$. Furthermore, the value of the parameter $\mathfrak{D}$ is expected to be nearly the same for all the models in Fig. 18. This is an attractive feature of the JT models compared to the vacancy models because it explains in a natural way the near equality of the observed $\mathfrak{D}$ values in Table III. Furthermore, the weakly perturbing vacancies can now be held responsible for changing the sign of $\alpha = \mathcal{E}/\mathfrak{D}$, i.e., for interchanging the crystal-field axes x and y (see Sec. IV C 1). Which specific configuration [(b), (c), or (d) in Fig. 18] accomplishes this must be checked by detailed calculations.

The Pb^- models (a) and (d) in Fig. 18 are structurally identical to the Sn^- (cubic) and Sn^- (tetrag) models shown in Figs. 7. The mere fact that one is able to propose such models here is again a positive feature of the JT models. The impossibility of even considering them in the framework of vacancy models was felt to be a great disadvantage.

Progress can be made by comparing the production, thermal, and optical properties of the Pb^- defects (Sec. V) with those of the Sn^- centers.[17] In making such a comparison it is quickly realized that Pb^- (1) has several pronounced features in common with Sn^- (tetrag), to wit: (i) The optical F-center—bleaching data strongly imply the existence of both a Pb^0 (1) (see Sec. V B) and a Sn^0 (tetrag) precursor center under electron trapping; (ii) the concentration of both centers is strongly enhanced by an x irradiation at 77 K if the crystal had been firstly x irradiated at RT; (iii) a V_K-center bleach be it an optical one (Sec. V C) or a thermal one (Sec. V A) substantially reduced the Pb^- (1) and Sn^- (tetrag) concentrations. In contrast, Pb^- (2) shares the Sn^- (cubic) properties: (i) No precursor centers under electron trapping exist; (ii) F- and V_K-center bleachings have only a small effect (a reduction mostly) on the concentration.

Consequently, within the framework of the JT models a good case can be made to associate the Pb^- (2) center with the Sn^- (cubic)-type model of Fig. 18(a) and the Pb^- (1) center with a Sn^- (tetrag)-type model in Fig. 18(d).

VII. CONCLUDING REMARKS

Through a detailed study of ESR spectra it has been established that several complex Pb^- defects are created in $KCl:Pb^{2+}$ by x irradiation above 220 K. The identification of the Pb^- $6p^3$ ion being the essential constituent of the defects was based on a careful analysis of the strongly anisotropic g tensor. It was found in particular that the Pb^- ground state requires a coupling scheme intermediate between LS and j-j. As a result the Pb^- ground-state splitting ($\sim 10^3$ cm^{-1}) in a crystal field of low symmetry is roughly two orders of magnitude larger than in the case of Sn^- (~ 10 cm^{-1}). The Sn^- $5p^3$ is rather well described by the LS-coupling scheme.

The substantial presence of orbital angular momentum in the fourfold-degenerate free-Pb^- ground state makes it highly probable that a Pb^- on an octahedral anion site will undergo a static orthorhombic Jahn-Teller distortion. This JT viewpoint, in contrast to the so-called vacancy-model viewpoint, is shown to be a fruitful one. Assuming the JT distortion to be dominant in all the observed Pb^- defects and assuming the nearby vacancies, instead of being the dominant perturbation as in the vacancy models, to merely exert an additional perturbation, permits in a straightforward way to understand the near constancy of the observed axial crystal-field parameter $\mathfrak{D}$ (Table III), and leads to Pb^- defect structures [Figs. 18(a) and 18(d)] which are similar to the Sn^- defects (Fig. 7). The latter conclusion is rather comforting because the similar impurity ions Sn^{2+} and Pb^{2+} in KCl then do indeed behave similarly, but the conclusion is not obvious at a first glance: The Sn^- ESR spectra are isotropic and axial while the Pb^- ones are orthorhombic. The existence of a dominant static JT effect in all the observed Pb^- defects is not unambiguously proven in this paper but the available data and their interpretation are, we believe, rather persuasive. Further experimental and theoretical work on Sn^- and Pb^- centers, also in matrices other than KCl, could be quite illuminating.

Two things were not discussed in this paper. First, no analysis of the ^{207}Pb hyperfine parameters (whose signs are not known) was attempted. Eventually an in depth theoretical analysis may prove to be very important in the determination of the precise Pb^- defect structures just as it was in the case of the complex Tl^0 defects in KCl.[19] A specific difficulty in such a theory, and also in connection with a theoretical treatment of the JT problem, could be that Pb^- may not be a stable ion in the free state but that it is stabilized by the Madelung field in the alkali halides. Second, no production mechanisms for the Pb^- defects were discussed. The general ideas put forward in connection with the production of the Sn^- centers[17] remain largely valid. The data obtained in this paper (Sec. V) underscore once more the central importance in these mechanisms of the mobility of the anion and cation vacancies in KCl above 220 K.

ACKNOWLEDGMENTS

The authors are indebted to J. Andriessen for communicating the results of his relativistic Hartree-Fock calculations and to A. Bouwen for his excellent experimental support. Discussions with A. Taurel, M. Billardon, B. Briat, and S. Lefrant were also very useful. The cooperation of I. Ursu and support from the I.I.K.W. (Interuniversitair Instituut voor Kernwetenschappen) and the N.F.W.O. (Nationaal Fonds voor Wetenschappelijk Onderzoek) are gratefully acknowledged.

---

[1] W. Kleeman, Z. Phys. 249, 145 (1971).

[2] W. Kleeman, L. Becker, and E. Grawe, in Proceedings of the Europhysics Topical Conference on Defects in Insulators, Canterbury, 1979, paper B24 (unpublished).

[3] F. Fisher, Z. Phys. 231, 393 (1970).

[4] K. Kojima, M. Mai, and T. Kojima, J. Phys. Soc. Jpn. 28, 1227 (1970).

[5] D. Lemoyne, J. Duran, M. Billardon, and Le Si Dang, Phys. Rev. B 14, 747 (1976).

[6] D. Lemoyne, J. Duran, and J. Badoz, in Proceedings of the

International Conference on Defects in Insulating Crystals, Gatlinburg, 1977 (unpublished), p. 262.

[7] A. Fukuda, Phys. Rev. B 1, 4161 (1970).

[8] V. Topa and B. Velicescu, Phys. Status Solidi 33, K29 (1969).

[9] V. Topa and M. Yuste, Phys. Status Solidi (a) 3, 131 (1970).

[10] M. Yuste and W. Bogusz, Phys. Status Solidi (b) 52, K133 (1972).

[11] B. Velicescu-Lupescu and V. Topa, Phys. Status Solidi (b) 55, 793 (1973).

[12] A. Ioan and V. Topa, Phys. Status Solidi (b) 101, 377 (1980); A. Ioan, V. Topa, and M. Giurgea, *ibid.* 89, 513 (1978).

[13] T. Tsuboi, Can. J. Phys. 57, 1510 (1979).

[14] W. Kleeman, Z. Phys. 214, 285 (1968).

[15] M. Billardon, B. Briat, V. Topa, and L. Taurel, in Magnetic Resonance and Related Phenomena, edited by I. Ursu, Proceedings of the Sixteenth Congress Ampére, Bucharest, 1971 (unpublished), p. 423.

[16] B. Lupescu and V. Topa, Rev. Roumaine Phys. 22, 503 (1977).

[17] F. Van Steen and D. Schoemaker, Phys. Rev. B 19, 55 (1979).

[18] See, e.g., W. Van Puymbroeck and D. Schoemaker, Phys. Rev. B 23, 1670 (1981), and references therein.

[19] E. Goovaerts, J. Andriessen, S. Nistor, and D. Schoemaker, Phys. Rev. B 24, 29 (1981).

[20] E. Goovaerts, A. Lagendijk, and D. Schoemaker, in Proceedings of the International Conference on Defects in Insulating Crystals, Gatlinburg, 1977 (unpublished); p. 153; E. Goovaerts, S. V. Nistor, I. Ursu, and D. Schoemaker, in the Fourth ISMAR-Ampére International Conference on Magnetic Resonance, Delft, 1980 (unpublished), p. 39.

[21] D. Schoemaker and J. L. Kolopus, Solid State Commun. 8, 435 (1970).

[22] C. J. Delbecq, D. Schoemaker, and P. H. Yuster, Phys. Rev. B 9, 1913 (1974); 7, 3933 (1973); 3, 473 (1971).

[23] F. Lüty, in *The Physics of Color Centers,* edited by W. B. Fowler (Academic, New York, 1968).

[24] J. P. Stott and J. H. Crawford, Phys. Rev. B 4, 639 (1971).

[25] E. U. Condon and G. H. Shortley, *The Theory of Atomic Spectra* (Cambridge University Press, Cambridge, England, 1967), p. 274ff.

[26] A. Abragam and B. Bleaney, *Electron Paramagnetic Resonance of Transition Ions* (Clarendon, Oxford, 1970), p. 650.

[27] J. Andriessen (private communication).

[28] J. P. Desclaux and N. Bessis, Phys. Rev. A 2, 1623 (1970).

[29] F. S. Ham, in *Electron Spin Resonance,* edited by S. Geschwind (Plenum, New York, 1972), p. 1.

[30] D. Schoemaker, Phys. Rev. B 7, 786 (1973).